Research Article

Huaixuan Feng, Xue-feng She*, Xiao-min You, Guang-qing Zhang, Jing-song Wang, and Qing-guo Xue

Carbothermal reduction of red mud for iron extraction and sodium removal

https://doi.org/10.1515/htmp-2022-0005
received June 29, 2021; accepted October 14, 2021

Abstract: In this work, the technology of carbothermic reduction was used to extract iron and remove sodium from red mud. The effect of various parameters like reduction time, temperature, and basicity on melting separation and de-alkalization was studied. At the optimum reduction temperature of 1,450°C, the basicity of 1.5, and reduction time of 12 min, the metallization rate and sodium removal reach 96.63 and 90.62%, respectively. Melting and separating conditions gradually improve with the temperature increasing from 1,350 to 1,450°C. At high basicity ($R = 2$), the condition of melting and separation is poor due to a large amount of $Ca_2Al_2SiO_7$ produced, which has a high melting point. Subsequently, in order to explore the aggregation state of iron ions under different basicities, the microstructure of pellets was observed by scanning electron microscopy. It was found that when the basicity is 1.5, the aggregation degree of iron particles significantly increases. X-ray diffraction (XRD) analyses of the reduced pellets indicated that at different basicities, the final phase composition of reduced pellets is mainly $Ca_2Al_2SiO_7$, which is the basic material for preparing cement materials and glass ceramics. Thus, the carbothermic-reduction method is a sustainable process for dealing with the Bayer bauxite residue.

Keywords: red mud, de-alkalization, carbothermic reduction, valuable element recycling, iron particle

1 Introduction

The Bayer process is one of the important methods or approaches to producing aluminum. It is reported that more than 90% of alumina is produced via the Bayer process. Thus, the Bayer bauxite residue accounts for a considerable percentage of the by-products of alumina extraction. For each ton of alumina produced, 1.0–1.5 tonnes of Bayer red mud is produced from different sources and processing parameters [1,2]. At present, it is reported that more than 2.7 billion tonnes of red mud have been accumulated in the world [3–6]. It contains aluminum, iron, and other valuable metals. Unfortunately, the average utilization factor of global red mud is only 15%, and for China it is 4% [7]. For the large-scale solution of the problem of red mud, the idea of extracting valuable metals first, and then using the residue in an integral unit is encouraged to completely recover or reuse all valuable components in red mud. However, on the one hand, the direct use of red mud for ironmaking has low economic benefits. On the other hand, the high content of alkalinity hinders the further use of red mud. Sintered brick and other wall materials produced from red mud generate alkali efflorescence that results in size expansion, cracking, and disintegration, thus decreasing the service life of buildings [8]. Its heavy metals and a certain amount of radioactive material poses a great challenge to the ecological environment. Moreover, red mud takes a large number of expenditures on stacking yard construction, maintenance, and management [9,10].

Thus, it is an urgent target to comprehensively use red mud and find a possible way for a nonhazardous treatment. As the red mud characters differ, different aspects were considered including valued metals recovered and de-alkalization for the materials of cement. Wang and Sun [11], Jiang et al. [12], and Yu et al. [13] reported that nickel and iron in red mud can be effectively recovered by direct reduction and magnetic separation. Alkaline metal salts were added, which enhanced the reduction of laterite ores, and the recovery rates of iron and nickel

* **Corresponding author: Xue-feng She,** State Key Laboratory of Advanced Metallurgy, University of Science and Technology Beijing, 100083 Beijing, China, e-mail: shexuefeng@ustb.edu.cn
Huaixuan Feng, Xiao-min You, Jing-song Wang, Qing-guo Xue: State Key Laboratory of Advanced Metallurgy, University of Science and Technology Beijing, 100083 Beijing, China
Guang-qing Zhang: School of Mechanical, Materials and Mechatronic Engineering, University of Wollongong, Wollongong, NSW 2522, Australia

were 93.77 and 95.25 wt%, respectively. Jayasankar and Ray [14] used thermal plasma technology to deal with red mud waste fines for recovering pig iron. They studied various process parameters like reductant, fluxes, and smelting time on the effect of iron recovery. Wang and Zhang [15,16] used the calcification-carbonization process to recover alumina and alkali from red mud. The process contained three steps: calcification transformation, carbonization transformation, and $Al(OH)_3$ leaching. They obtained the final residue, and Na_2O contents of the alumina below 0.3 and 46.5% were extracted, which can be used for cement material. Although some progress has been achieved, these methods are complicated and a great amount of $Al(OH)_3$ was consumed.

In this work, the carbothermic reduction of Bayer red mud was performed to recover valued elements and dealkalization. At enough content of carbon, iron oxide in red mud can be reduced to metallic iron, Na_2O can be reduced to sodium vapor, and the residue can be transformed to gehlenite. First, the effect of temperature and CaO content on pellet melting separation was investigated. Then, the metallization rate and sodium removal rate of pellets before and after reduction were obtained by using X-ray fluorescence (XRF). X-ray mapping via scanning electron microscopy (SEM) for elements Fe and Na in the reduction process was used to study the state of aggregation. The residual phase composition was established by X-ray diffraction (XRD). The main objectives of this research are to investigate the behavior of red mud in the carbothermic reduction and melting separation process and to remove sodium.

2 Experiment materials and methods

2.1 Raw materials

The red mud used in this experiment came from a steel plant in China. The XRF analysis results of red mud in this work are shown in Table 1. As can be seen, the Al_2O_3 and Fe_2O_3 contents were relatively high, 20.28 and 33.21%, respectively, which indicated that the red mud was the residue formed in the Bayer process [17]. It is worth noting that the content of Na_2O was 8.63%. XRD analysis was used to determine the phases, and the results are shown in Figure 1. The main phases in the red mud were hematite (Fe_2O_3), goethite (FeOOH), sodalite ($1.06Na_2OAl_2O_31.60SiO_21.60H_2O$), gibbsite ($Al(OH)_3$), quartz ($SiO_2$), and the

Table 1: Chemical composition of the red mud (wt%)

Na_2O	Al_2O_3	SiO_2	CaO	TiO_2	Fe_2O_3
8.63	20.28	16.66	3.84	3.92	33.21

iron element in the red mud existed in the form of hematite and goethite. In addition, the particle size of red mud was tiny (0.088–0.25 mm), which was beneficial for the reduction treatment [18]. The scanning electron microscopy image of the red mud is also shown in Figure 2, revealing that the surface of red mud agglomerates was made of many small compact particles that were amorphous and irregular. Pulverized anthracite coal was used as a reductant. The chemical composition of the anthracite coal is listed in Table 2, which indicated that it was high in fixed carbon and relatively low in ash and sulfur.

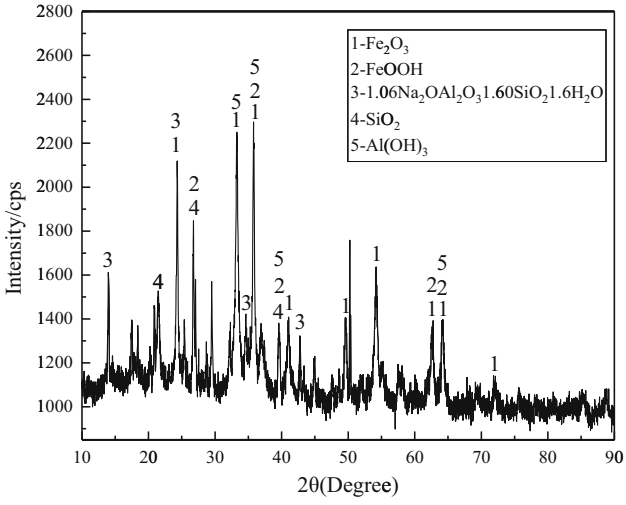

Figure 1: XRD analysis of the Bayer red mud.

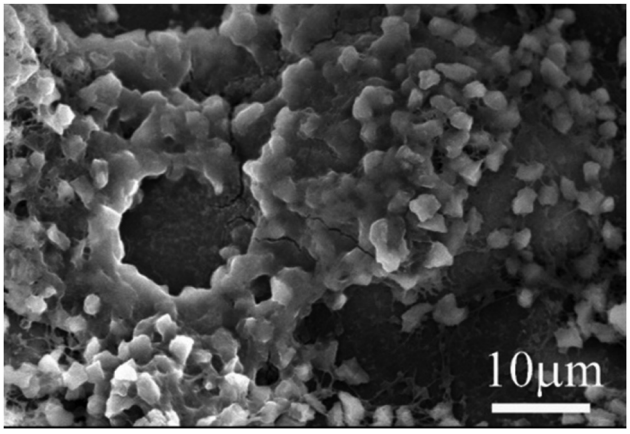

Figure 2: Microstructure of the Bayer red mud.

Table 2: Chemical composition of anthracite (wt%)

Proximate analysis				Ash analysis					S	P
FCd	Vd	Ad	Mad	SiO_2	Al_2O_3	Fe_2O_3	CaO	MgO		
81.05	5.98	10.14	2.83	42.79	35.70	2.82	7.89	0.92	0.32	0.06

2.2 Experimental methods

Before being crushed and screened to <200 μm, the red mud and anthracite coal were dried in an oven at 105°C for 48 h. Then, these materials were fully mixed with CaO as shown in Table 3. Furthermore, the mixture was pressed at 20 kN for 2 min into ~7.0 g cylindrical tablets of 15 mm diameter and 10 mm height for the reduction experiment [19].

Basicity, time, and temperature were considered in the present work. The basicities of the pellets were set as 1.0, 1.5, and 2.0, and the temperature of the experiment was varied in the range of 1,350–1,450°C (50°C increments). First, the effect of temperature on melting and separating the pellet was investigated with the basicity fixed at 1.5. The amounts of anthracite coal in the current study were 1.5 times larger than the stoichiometric needed to ensure the complete reduction of iron oxides. The muffle furnace was first preheated to a temperature of 1,350°C; then, the carbon-bearing pellets were put into the furnace with the holding time set to 2–12 min. After the reaction, the pellets were taken from the furnace and cooled to ambient temperature under an argon atmosphere. Then, the preheating temperatures were set at 1,400 and 1,450°C, and the experiment process was repeated as before.

Second, in order to explore the influence of basicity on the experiment, different alkalinities were set up for experimental analysis. The value of basicity in the experiment was obtained by calculating the mass ratio of calcium oxide and silicon dioxide. Since the mass of silica in the red mud was more than that of calcium oxide, calcium oxide was added to adjust the alkalinity to 1.0–2.0.

Table 3: The main composition of carbon-bearing pellets under different conditions (wt%)

	Red mud	CaO	Anthracite coal
T = 1,350°C	74.24	15.74	10.02
T = 1,400°C	74.24	15.74	10.02
T = 1,450°C	74.24	15.74	10.02
R = 1.0	79.11	10.21	10.68
R = 1.5	74.24	15.74	10.02
R = 2.0	69.93	20.63	9.44

To avoid the energy deficiency at low temperatures, the furnace temperature was set at 1,450°C. The basicity of the pellets in the experiment varies from 1.0 to 2.0. One of the reduced pellets was cut from the middle, and then were mounted in epoxy resin, polished, sprayed by the carbon film for the cross-sectional observation by SEM-EDS. Moreover, X-ray mapping was used to observe the distribution density variation of the element Na in different positions of the pellets with increasing reduction time. The other reduced pellet was ground for XRD analysis and chemical analysis.

The metallization rate (η_{Fe}) and sodium removal rate (ε) were adopted as evaluation indices of the process of carbothermal reduction.

The metallization rate of iron components (η_{Fe}) can be expressed as

$$\eta_{Fe} = M_{Fe}/T_{Fe} \times 100\%, \quad (1)$$

where M_{Fe} is the metallic iron content in the reduced pellets and T_{Fe} is the total iron content in reduced pellets.

The sodium removal rate of pellets can be calculated as

$$\varepsilon = \frac{m_1\alpha - m_2\beta}{m_1\alpha} \times 100\%, \quad (2)$$

where m_1 is the initial mass of the pellet, g; m_2 is the mass of pellets after reduction, g; α is the content of Na_2O in the initial pellets; and β is the content of Na_2O in the pellets after reduction.

3 Results and discussion

3.1 Effect of temperature on the reduction and melting separation

One of the purposes of studying red mud was to recycle valued elements. In this study, carbothermal reduction at high temperatures was used for separating iron and slag. The morphology of pellets was discussed with respect to temperature first, as shown in Figure 3.

It was clearly seen that the morphology of the pellets was different from the temperature change.

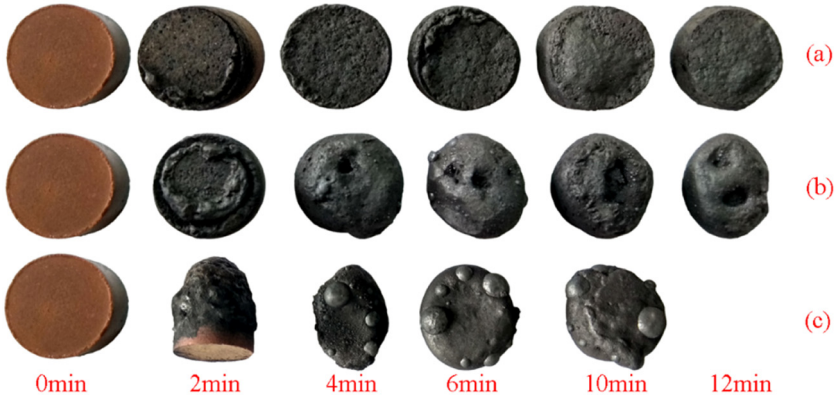

Figure 3: The melting and separation of red mud at different times and temperatures: (a) 1,350°C, (b) 1,400°C, and (c) 1,450°C.

When the temperature increased, the amount of carburizing gradually increased, and the melting point of iron decreased, which was easy to separate from the slag. At 1,350°C, the condition of melting separation was poor, and the slag and iron cannot be completely separated. With the temperature further increasing, the iron nugget and slag can separate well at 1,450°C. The iron element exists in the form of an iron bead, scattered on the edge of the pellet, and the diameter can grow up to 5 mm. At 1,450°C, the shape of pellets at 6 and 10 min were almost the same, indicating that the melting and separation were completed at 6 min. In addition, in order to study the metallization rate of the pellets after melting and separation, XRF was used to determine the content of Fe^{2+} and TFe. According to equation (1), the metallization rate (ε) was calculated and the results are shown in Figure 4.

Figure 4 shows that the temperature greatly influences the metallization rate. The metallization rate increased initially from 78.59 to 96.63% as the temperature increased from 1,350 to 1,450°C. Afterward, the metallization rate was basically unchanged when the reduction time reached 12 min. Thus, a temperature of 1,450°C was an advantage for the red mud reduction and melting separation.

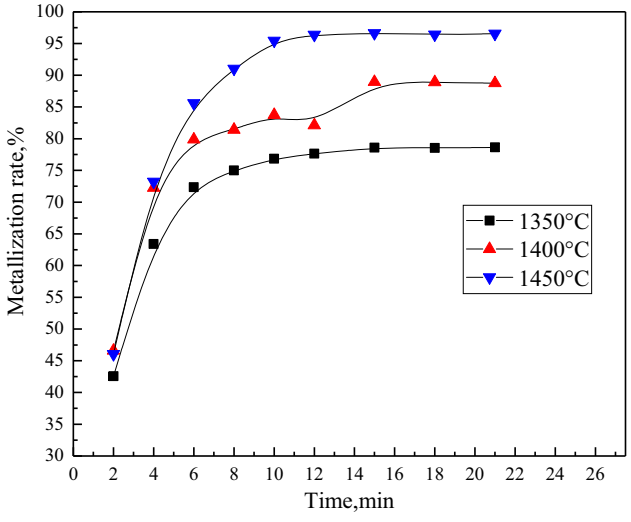

Figure 4: Effect of temperature on the metallization rate of pellets.

In the smelting reduction separation process, the melting of reduced iron and slag were the decisive factors. The melting temperature of reduced iron was mainly related to carburization, while the melting of slag was mainly related to composition. Since the composition of slag had not changed, the temperature of reduced iron became the main factor that limited the melting and separation of the pellets. At 1,350°C, because of the low temperature and insufficient iron carburization, the iron element was difficult to melt, thus the slag and iron could not be completely separated. As the temperature increased, the carburizing process sped up, resulting in the melt of metallic iron. Under the high heating temperature, the fluidity of the slag and iron was improved, and the separation was more thorough. Due to the difference in density, the metallic iron sank downward while the slag moved upward. According to Wang et al. researched [20], in the initial stage of isothermal thermal reduction, the content of FeO in the slag was related to its surface tension, i.e., as the FeO content decreased, the surface tension of the slag gradually increased. Therefore, the slag could not gather on the upper part of the iron and would move to the side of the iron.

3.2 Effect of basicity on reduction and melting separation

In this section, different basicity on the influence of melting and separation were studied. Results were shown in Figure 5 with the basicity of the pellets set as 1.0, 1.5,

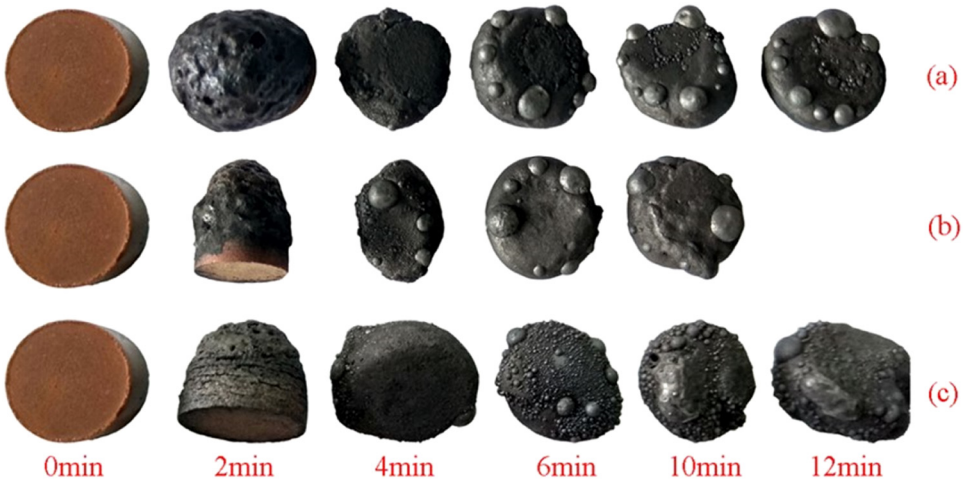

Figure 5: The melting and separation of red mud at different times and basicities at a temperature of 1,450°C: (a) R = 1.0, (b) R = 1.5, and (c) R = 2.0.

and 2.0. It could be concluded that basicity has an important effect on the iron-slag melting separation of the pellets. As the basicity increases from 1.0 to 1.5, the separation effect of slag and iron was remarkable. Metal iron aggregated and grew to form iron beads. When the basicity was 1.5 and the reduction time was 4 min, the diameter of the metallic iron in the pellets could reach about 6.5 mm. When the reduction time was prolonged to 6 and 10 min, the pellet melting effect was basically the same, indicating that the melting was over at 6 min. While the basicity increased to 2.0, as the reduction time increased, a large number of fine iron particles gradually precipitate out, scattered on the surface of the slag. The condition of iron-slag melting separation of the pellet was poor. It may be due to the fact that the fluidity in the slag was poor, resulting in the decrease of the rate of mass transfer so that the iron produced by the reduction fails to accumulate.

It is well known that can play the role of network modifier in the slag [21–23]. $[SiO_4]$-tetrahedral and $[AlO_4]$-tetrahedral could be formed by SiO_2 and Al_2O_3 in the molten slag, which was combined through the bridging oxygen (O0) [24,25]. With the increasing content of CaO, the availability of free oxygen ions (O_2^-) in the molten slag was increased. Then, O_2^- could react with O0 in the network structure to form nonbridging oxygen (O^-), which simplified the structure of the melt. In this way, the viscosity of slags decreased and the fluidity was improved. The mass transfer conditions were improved, promoting the separation of iron and slag.

However, when the basicity of the pellet increased to 2.0, iron and slag could not separate well. It might be ascribed to the fact that a large amount of gehlenite was formed at the high content of CaO, which had a high melting point [26]. Thus, the mass transformation got worse when the basicity was 1.5.

Figure 6 shows the metallization rate under different basicities. The metallization rate of the reduced pellet with a basicity of 1.5 was higher than that at 1.0 and 2.0. Moreover, the metallization rate of the pellet with a basicity of 1.5 was 96.37% when the reduction time was 12 min, remaining stable for the rest of the time, indicating that the carbothermal reduction process was completed. Considering the melting separation condition and the metallization rate of the pellet synthetically, the optimal reduction temperature and basicity were 1,450°C and 1.5, respectively.

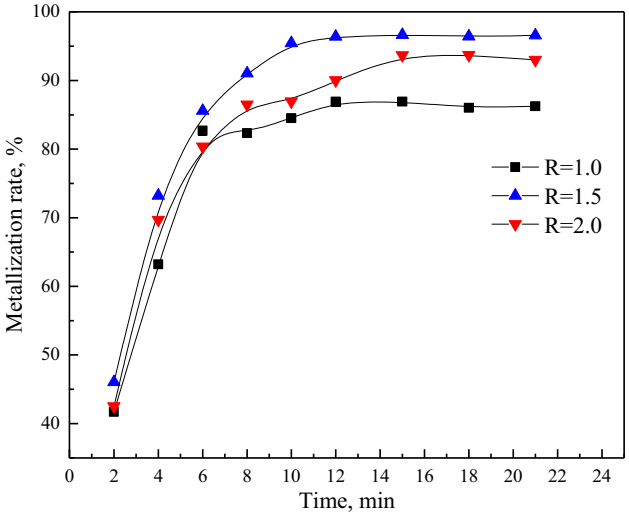

Figure 6: Effect of basicity on the metallization rate of pellet at 1,450°C.

The iron mineral reduction of red mud included the reduction of iron oxides and the growth of metallic iron. Figure 5 shows that the iron oxide in the red mud could be reduced to metallic iron. Therefore, the main factor influencing the microstructure of the pellet was the grain size of metallic iron, which was the premise of the liberation of iron shot [26]. Thus, in this work, we approaced from a microscopic perspective of pellets under different basicities, which is shown in Figure 7.

It was clearly seen that at a basicity of 1.5, the growth of metallic iron particles (light white area) was enhanced significantly with the diameter size above 80 μm. At a basicity of 1.0 (Figure 7(a)), most metallic iron particles were isolated from each other, while there were some sheets that appeared as the basicity increased to 1.5 (Figure 7(c)). In addition, as shown in Figure 7(c) and (d), adjacent iron particles gradually aggregated and grew to form a sheet, which was consistent with the results of Fan and Ni [26]. However, when the basicity increased from 1.5 to 2.0, it was obvious that the iron particles evenly dispersed on the surface of the pellet without aggregation. small amounts of big particles was found at a basicity of 2.0, as shown in Figure 7(e). Thus, it was testified that due to an excessive formation of gehlenite, the mass transfer in the pellets got worse. Furthermore, comparing Figure 7(a), (c), and (e) with (b), (d), and (f), the metallic iron particles mainly assembled in the edge part around the pellets, and the center of the pellet was in disperses state.

3.3 Phase transformation of the pellet under different basicities and temperatures

The phase compositions of the slag after reduction under different basicities are shown in Figure 8. Figures 1 and 8 show that the peaks of hematite and goethite disappear

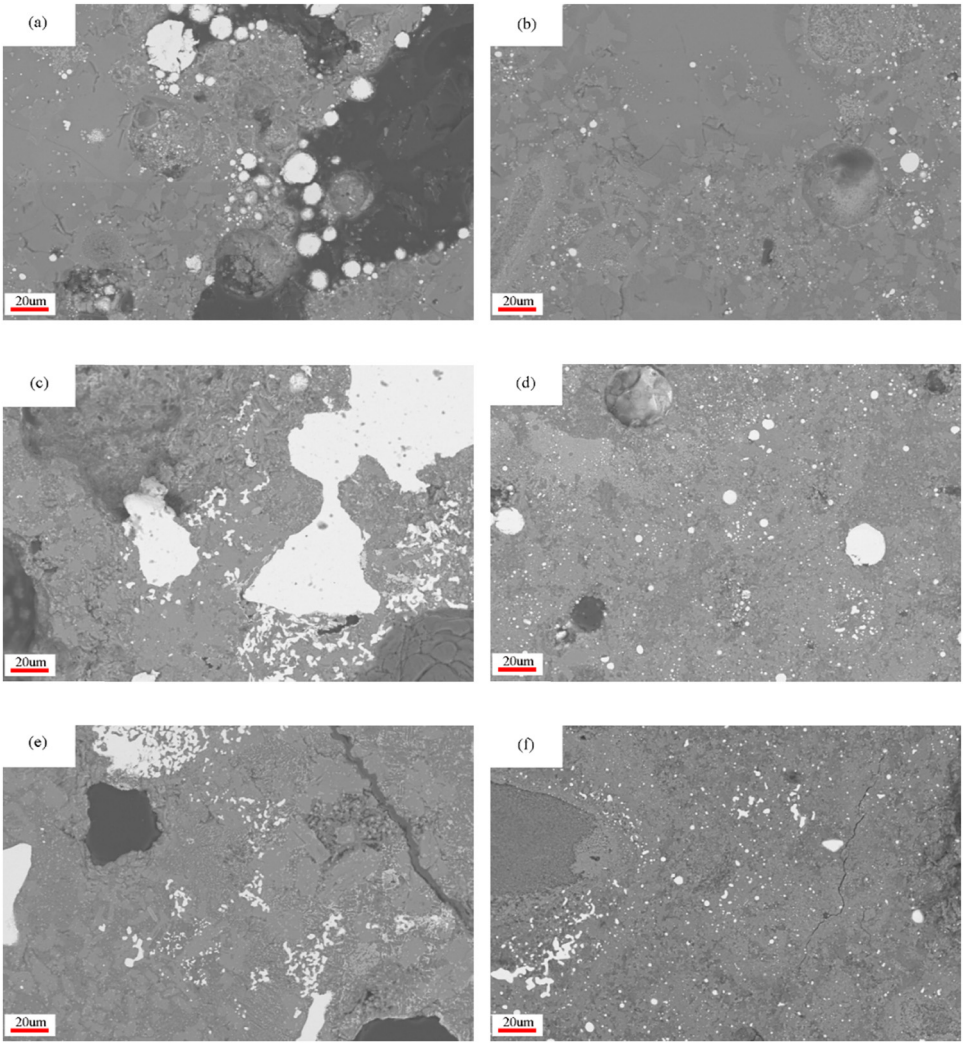

Figure 7: Microstructure of reduced pellets of the red mud under different reduction conditions: (a and b) R = 1.0, (c and d) R = 1.5, and (e and f) R = 2.0.

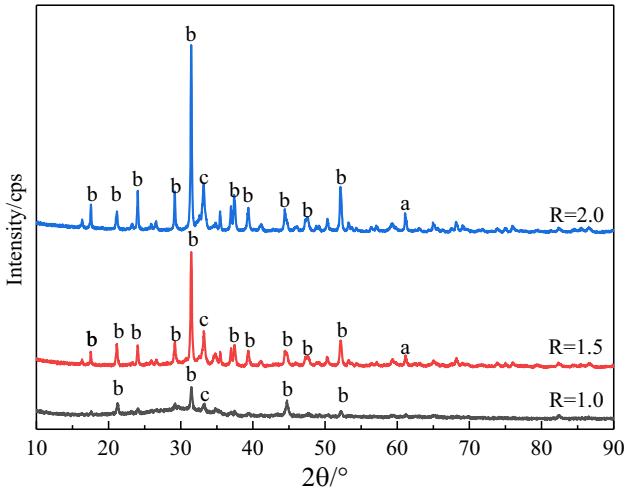

Figure 8: The phase compositions of the slag after reduction under different basicities: (a) $NaCaAlSi_2O_7$; (b) $Ca_2Al_2SiO_7$; and (c) $CaTiO_3$.

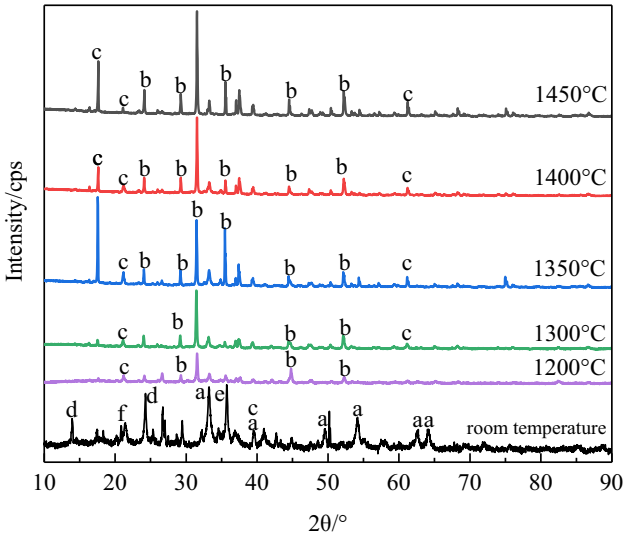

Figure 9: XRD pattern of the slag at different temperatures: (a) Fe_2O_3; (b) $Ca_2Al_2SiO_7$; (c) $NaCaAlSi_2O_7$; (d) sodalite; (e) $Al(OH)_3$; and (f) SiO_2.

and the peaks of $Ca_2Al_2SiO_7$ and $NaCaAlSi_2O_7$ appear in the reduced pellets. The results indicate that the iron minerals in the original pellets were reduced and transformed into metallic iron. The peaks of sodalite, gibbsite, and quartz were not detected. $Ca_2Al_2SiO_7$ was the main phase in the reduced pellets, which was one of the components of cement materials and glass-ceramics [27,28]. The composition of pellets under different basicities had not changed and there were two phases in the pellets. With the increase of the basicity from 1.0 to 1.5, the content of different phases increased, which might be the reason that CaO changed the mass transfer conditions in the slag thereby increasing the mass transfer rate in the slag. It was obvious that the content of $Ca_2Al_2SiO_7$ was increased with the basicity increase from 1.0 to 2.0. As discussed above, a large amount of $Ca_2Al_2SiO_7$ improved the melting point of the whole molten slag, resulting in the melting and separation getting worse, which was in accordance with the result of Figure 6.

Likewise, to investigate the relationship between the reduction process and temperature, XRD was used to study the phase transformation of the slag, and the results are shown in Figure 9. It is obvious that temperature had an important effect on the reduction of the pellets. When the temperature was increased to 1,200°C, diffraction peaks of hematite (Fe_2O_3) vanished,

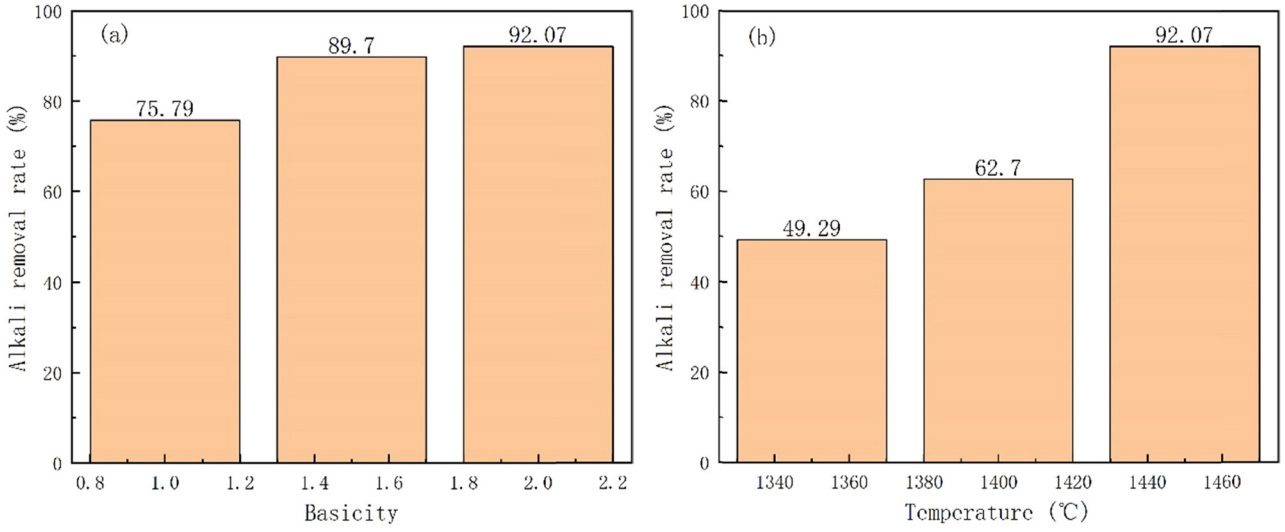

Figure 10: Effect of temperature and basicity on the alkali removal rate: (a) different basicities, T = 1,450°C and (b) different temperatures, R = 1.5.

indicating that the reduction process of the pellet was complete. As suggested in the Ellingham diagram [29], there were three steps in the reduction of iron oxides: $Fe_2O_3 \rightarrow Fe_3O_4 \rightarrow FeO \rightarrow Fe$. However, as the temperature gradually increased from 1,350 to 1,450°C, the peak of hematite (Fe_2O_3) did not appear in the XRD result, which was not consistent with the result of the metallization rate (Figure 4). This was due to the fact that during the reduction of the pellets, the iron grade in the slag gradually decreased, and thus the content of iron oxide was too small to be detected by XRD. In addition, it could be seen that the main components of slag at high temperatures are $Ca_2Al_2SiO_7$ (C2AS) and a small part of $NaCaAlSi_2O_7$. With the increase of temperature, the sodium salt gradually decreased while the content of C_2AS gradually increased. The detailed discussion is described in Section 3.4.

3.4 De-alkalization

The production of building materials (such as cement, brick, and road base material) with the bauxite residue was a direct, simple, economical, and quick way to consume a large amount of the substance [30,31]. However, the component of red mud that was used for cement was strictly controlled. If the alkali content of the cement was too high [32], an alkali-aggregation reaction would occur

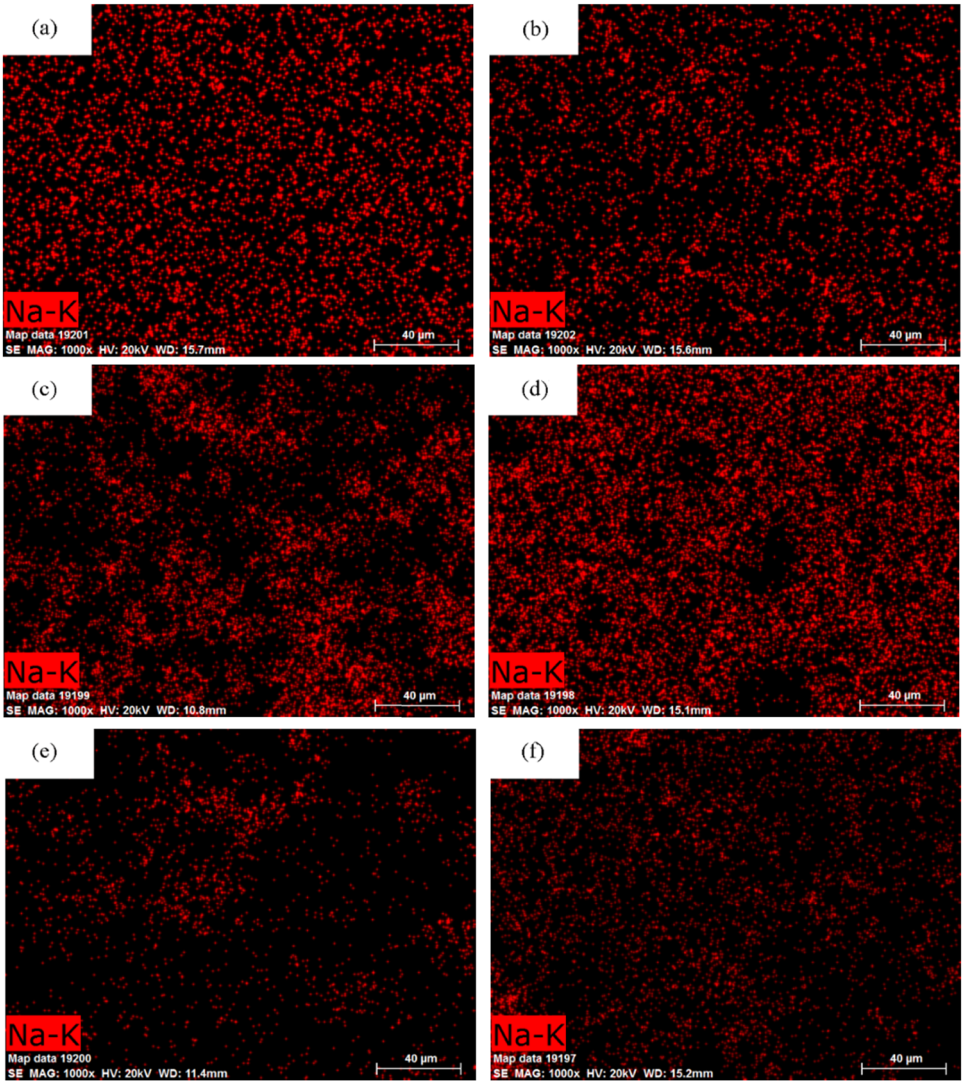

Figure 11: X-ray mapping analysis via SEM of Na in the reduction process (R = 1.5, T = 1,450°C) (a and b) 2 min, (c and d) 6 min, (e and f) 15 min.

in the concrete, resulting in low strength and inadequate durability, which might cause serious project quality or safety issues and accidents [16]. Therefore, from the perspective of waste utilization, this section studied the removal efficiency of sodium from the red mud by carbothermal reduction.

As shown in Figure 10, the removal rate of alkali increased with the increase of temperature and alkalinity under different conditions. The temperature was more important than the basicity for sodium removal. At a fixed basicity, the temperature was increased by 100°C, and the alkali removal rate was increased from 49.29 to 90.62%. When the basicity was increased from 1.0 to 2.0, the change range of the alkali removal rate was relatively small (75.79–92.07%).

The reactions of sodium in red mud are shown in equations (3)–(5). Sodium oxide reacts with silica to form sodium silicate. It was more important than calcium oxide being used as an additive. Excess carbon reduced the sodium in sodium silicate and was released as sodium vapor. The calcium silicate produced in equation (4) reacted with the alumina in the red mud. These results basically corresponded to the XRD patterns. However, in Figures 8 and 9, a part of sodium existed as $NaCaAlSi_2O_7$ because the Ca element in $Ca_2Al_2SiO_7$ was replaced by the Na element to form sodalite, and thus sodium could not be completely removed [33]. Meanwhile, from the thermodynamics viewpoint, equation (5) is an endothermic reaction. As the temperature increased, the reaction proceeded in the direction of the positive reaction, thereby promoting the removal of sodium. The removal rate improved with an increase in basicity due to the improvement in the mass transfer. Therefore, the alkalinity content in the red mud could be reduced to a certain level, which provided a convenient condition for further utilization:

$$Na_2O + SiO_2 = Na_2SiO_3, \quad (3)$$

$$xC + xCaO + Na_2SiO_3 = xCO(g) + 2Na(g) + Ca_xSiO_3, \quad (4)$$

$$CaSiO_3 + Al_2O_3 = Ca_2Al_2SiO_7. \quad (5)$$

Furthermore, in order to investigate the initial position of sodium removal and the time the steady state was reached, X-ray mapping via SEM was used for the pellets ($R = 1.5$, $T = 1{,}450$°C) with the reduction time lasting for 2, 6 min, and 15 min. The center and right edge of the projectile were selected as the observation positions. The scanning results are illustrated in Figure 11, and the concentration of sodium elements measured in different regions is shown in Figure 12. The detailed operation for measuring the element content by the LA-ICP-MS system was given in the previous article.

As can be clearly seen from Figures 11 and 12, the concentration of sodium gradually decreased with the increase of the reduction time. At 2 min, there was no obvious change in the sodium concentration between the edge and center of the pellets. However, the concentration of sodium at the center of pellets was significantly lower than that at the edge as the reduction time increased to 6 min, showing a clear concentration gradient. It was speculated that the carbothermal reduction started at the center of the pellet, and the generated sodium vapor flowed out from the gap of the pellets, resulting in the difference in the removal rate at different positions. Furthermore, when the reduction time was increased to 15 min, they appeared almost the same distribution at low concentration, indicating that the reduction process of sodium had been completed and reached a steady state.

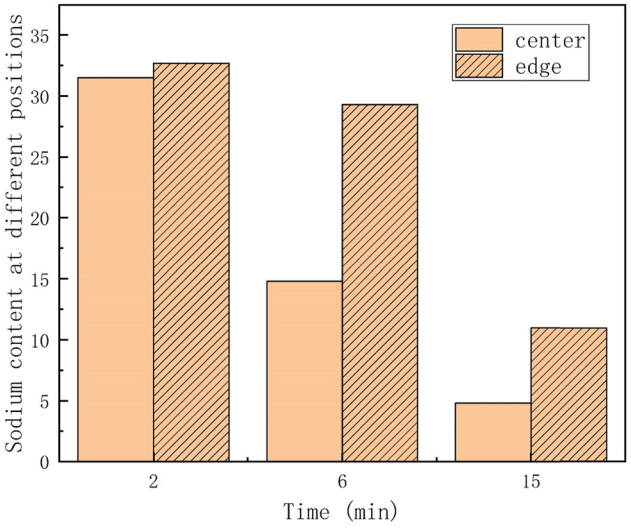

Figure 12: Sodium content at different positions of the pellets ($R = 1.5$, $T = 1{,}450$°C).

4 Conclusion

In this work, the carbothermic reduction was used to extract iron and remove alkali from the red mud. The effect of different parameters like reduction time, temperature, and basicity on melting, separation, and de-alkalization was studied, and some conclusions can be drawn as follows:

(1) At a basicity of 1.5 and temperature of 1,450°C, the melting and separation of slag iron in the red mud produced by the Bayer method was thorough, the metallization rate reached 96.63%, and the sodium removal rate reached 90.62%.

(2) At 1,450°C, the melting and separation condition gradually improved with increasing basicity from 1.0 to 1.5. However, when the basicity further increased to 2.0, the condition did not improve. Because high basicity results in a large amount of gehlenite, it causes an increase in the melting point of the system. Thus, the melting and separation were poor.
(3) The product after carbothermal reduction of the red mud is mainly $Ca_2Al_2SiO_7$, which can be used as cement materials and glass-ceramics in the construction industry.
(4) The concentration of sodium at the center of pellets was significantly lower than that at the edge when the reduction time increased to 6 min, showing a clear concentration gradient.

Acknowledgements: This work was supported by the National Key Research and Development Program of China (2019YFC1905703), and the National Natural Science Foundation of China (No. 51874029), which is acknowledged.

Funding information: This work was supported by the National Key Research and Development Program of China (2019YFC1905703), and the National Natural Science Foundation of China (No. 51874029).

Author contributions: Jing-song Wang and Xue-feng She were engaged in research on the recycling of solid waste from iron and steel metallurgy.

Conflict of interest: Authors state no conflict of interest.

References

[1] Liu, D. Y. and C. S. Wu. Stockpiling and comprehensive utilization of red mud research progress. *Materials*, Vol. 5, 2012, 1232–1246.
[2] Qi, C. Aluminum industry and its waste treatment. *World Nonferrous Metals*, Vol. 1, 2019, id. 2.
[3] Liu, Z. B. and H. X. Li. Metallurgical process for valuable elements recovery from red mud – a review. *Hydrometallurgy*, Vol. 155, 2015, pp. 29–43.
[4] Paspaliaris, I. and A. Karalis. Metallurgical process for valuable elements recovery from red mud-A review. *Light Met*, Vol. 32, 1998, id. 35.
[5] Zhang, R. and S. L. Zheng. Recovery of alumina and alkali in Bayer red mud by the formation of andradite-grossular hydrogarnet in hydrothermal process. *Journal of Hazardous Materials*, Vol. 189, 2011, pp. 827–835.
[6] Adamson, A. N., E. J. Bloore, and A. R. Car. Extractive metallurgy of aluminum. *Extractive Metallurgy of Aluminium*, Vol. 1, 1963, id. 75.
[7] Zhang, T. A., and Y. X. Wang, Comprehensive utilization of red mud: current research status and a possible way forward for non-hazardous treatment. The Minerals, Metals & Materials Society, 2018, 135.
[8] Zhuo, R. F. *Research on the preparation of CBC road base material from red mud*, Kunming University of Science and Technology, Kunming, 2009.
[9] Liu, W. C. and J. K. Yang. Review on treatment and utilization of bauxite residues in China. *International Journal of Mineral Processing*, Vol. 93, 2009, pp. 220–231.
[10] Agrawal, A., K. K. Sahu, and B. D. Pandey. Solid waste management in non-ferrous industries in India. *Resources, Conservation and Recycling*, Vol. 42, 2004, pp. 99–120.
[11] Wang, X. P. and T. C. Sun. Feasibility of co-reduction roasting of a saprolitic laterite ore and waste red mud. *International Journal of Minerals, Metallurgy and Materials*, Vol. 25, 2018, pp. 591–597.
[12] Jiang, M., T. C. Sun, and Z. G. Liu. Chemically and mechanically isolated nanocellulose and their self-assembled structures. *International Journal of Mineral Processing*, Vol. 123, 2013, pp. 32–40.
[13] Yu, W., T. C. Sun, Q. Cui, C. Y. Xu, and J. Kou. Effect of coal type on the reduction and magnetic separation of a high-phosphorus oolitic hematite ore. *ISIJ International*, Vol. 55, 2015, pp. 536–543.
[14] Jayasankar, K. and P. K. Ray. Production of pig iron from red mud waste fines using thermal plasma technology. *International Journal of Minerals, Metallurgy and Materials*, Vol. 19, 2012, pp. 679–684.
[15] Wang, Y. X. and T. A. Zhang. Recovery of alkali and alumina from bauxite residue (red mud) and complete reuse of the treated residue. *Journal of Cleaner Production*, Vol. 188, 2018, pp. 456–465.
[16] Wang, Y. X. and T. A. Zhang. Reaction behaviors and amorphization effects of titanate species in pure substance systems relating to Bayer digestion. *Hydrometallurgy*, Vol. 171, 2017, pp. 86–94.
[17] Hu, J.B. *Research on synthesis of calcium aluminate smelting and reduction red mud* [Degree dissertation], Wuhan University of Science and Technology, Wuhan, 2010.
[18] Yang, W. *Research on recovery of iron alumina from red mud* [Master thesis], Central South University, Changsha, 2012.
[19] She, X. F. and J. S. Wang. Mechanism of reduction process about rare earth Bayan Obo complex iron by graphite. *Chinese Journal of Rare Metals*, Vol. 41, 2017, id. 73.
[20] Ishiwata, N., Y. Sawa, and H. Hiroha. Investigation of reduction and smelting mechanism in the Hi-QIP process. *Steel Research International*, Vol. 80, 2009, id. 523.
[21] Feng, C. and M. S. Chu, Effects of CaO/SiO_2 on viscous behaviors and structure of $CaO\text{-}SiO_2$-11.00wt%MgO-11.00wt% Al_2O_3-43.00wt%TiO_2 slag systems. *ISIJ International*, Vol. 59, 2019, pp. 31–38.
[22] Zhou, L. J. and W. L. Wang. Molecular detection and genetic identification of Babesia bigemina, Theileria annulata, Theileria orientalis and Anaplasma marginale in Turkey. *Metals and Materials International*, Vol. 21, 2015, pp. 126–134.
[23] Liang, D. and Z. M. Yan. Transition of blast furnace slag from silicate-based to aluminate-based: structure evolution by molecular dynamics simulation and raman spectroscopy. *MMTB*, Vol. 48, 2017, pp. 573–581.

[24] Gao, Y. M., S. B. Wang, C. Hong, X. J. Ma, and F. Yang. Effects of basicity and MgO content on the viscosity of the SiO2-CaO-MgO-9wt%Al2O3 slag system. *International Journal of Minerals, Metallurgy and Materials*, Vol. 21, 2014, pp. 353–362.
[25] Kim, J. B. and I. l. Sohn. Effect of SiO2/Al2O3 and TiO2/SiO2 ratios on the viscosity and structure of the TiO2–MnO–SiO2–Al2O3 welding flux system. *ISIJ International*, Vol. 54, 2014, pp. 2050–2058.
[26] Fan, D. C. and W. Ni. Orthogonal experiments on direct reduction of carbon-bearing pellets of bayer red mud. *International*, Vol. 22, 2015, id. 686.
[27] Yang, J. K. and D. D. Zhang. Local knowledge, science, and institutional change: the case of desertification control in Northern China. *Materials Science and Technology*, Vol. 13, 2015, pp. 616–633.
[28] Yang, J. K. and J. Hou. Pilot-scale production and industrialization of the no-fired bricks from red mud in aluminum industry.*Environmental Engineering*, Vol. 25, 2006, id. 52.
[29] Zhan, J. Y., Principles of nonferrous metallurgy. Metallurgical Industry Press, Beijing, 2004, 208.
[30] Ding, Y. G. and Wang J. S.. Research on reduction kinetics of carbon-bearing pellets of BOF dust and slud. Vol. 10(S1), 2010, pp. 73–77.
[31] Pappu, A., M. Saxena, and S. Asolekar. Solid wastes generation in India and their recycling potential in building materials. *Building and Environment*, Vol. 42, 2007, pp. 2311–2320.
[32] Bi, S. W. The bayer process produces alumina. Metallurgical Industry Press, Beijing, 2007.
[33] Wang, Y. C., F. Dong, and B. F. Wang. Study on crystalline phases of free fluoride mould powder. *Inner Mongolia Petrochemical Industry*, 2006.